INTERNATIONAL JOURNAL OF PRECISION ENGINEERING AND MANUFACTURING

Modified Adaptive Input Shaping for Maneuvering Cranes Using a Feedback MEM Gyroscope with Null Drift

Joaquim M. Veciana[1,#], Salvador Cardona[1], Pau Català[1]

1 Department of Mechanical Engineering, Universitat Politècnica de Catalunya, ETSEIB, Diagonal 647, Barcelona, Spain, 08028
Corresponding Author / E-mail: joaquim.maria.veciana@upc.edu, TEL: +34-93-4016718, FAX: +34-93-4015813

KEYWORDS : Residual vibration; Residual response; Vibration control; Command shaping; Input shaping; Crane control; Adaptive identification

This paper presents an adaptive algorithm to reduce residual vibrations when the feedback sensor used has the drawback of having null drift along the time. The adaptive approaches are useful to deal with large variations of the system parameters at each maneuver, such as it occurs in cranes. For the feedback sensor, the use of inertial measurement units such as Micro-Electro-Mechanical Systems (MEMS) is increasingly extended because of their cost, size, robustness and power consumption. However, the effectiveness of the adaptive input shaping algorithms is compromised because of this drift, which is a commonly raised issue in this kind of devices. For a standard crane application, this major drawback could be avoided with a frequent time-basis calibration of the sensor, but it is not a feasible solution. The study presented in this manuscript focuses on the development of an automatic compensation of this drift to obviate such frequent calibrations. It is based on a non-asymptotic algebraic identification technique, which has the advantage of not requiring initial conditions and having a short convergence time. The new formulation uses the Zero-Vibration (ZV) input shaper technique, and the null drift is added to the algorithm as a new parameter to be identified. The proposed method has been particularized for single maneuvers of cranes with a gyroscope as feedback sensor, in a real time scenario. Experimental results show the efficacy of the method with its application to a scaled crane test platform.

1. Introduction

Motion control for rest-to-rest maneuvers in lightly-damped oscillation systems has been one of the main areas of focus for the development of residual vibration reduction [1-3], and cranes have been one of the widely addressed industrial applications [4-11]. In the case of standard cranes, the cable length and the inertia of the payload will change between maneuvers and, hence, a large variation of the system parameters is foreseen. Classic methods to reduce residual vibrations such as the built-in robustness methods derived from the ZV [12-15] input shaping have been developed to overcome light uncertainties when the system parameters are estimated: The zero-vibration and derivative (ZVD) and successive derivatives (ZVDD, …) [13] provide better performance with the drawback of longer command duration, and the so-called extra-insensitive (EI) and multi-hump input shapers [16,17] allow some residual vibration with shorter command durations. Nevertheless, to cope with a large system parameters variation, learning input shaping and adaptive input shaping become relevant. Learning input shaping (LIS) [18,19] provides a solution after several repetitive maneuvers, while the adaptive input shaping (AIS) [20-24] requires only one, resulting in a better approach for single maneuvers on cranes. Both of them estimate the system parameters by including in their algorithms the output response measured through a feedback sensor.

Due to the nature of our application, the feedback sensor must be close to the payload and, therefore, it is recommended the use of inertial measurement units (IMU), like accelerometers or gyroscopes. Within them, the use of Micro-Electro-Mechanical Systems (MEMS) is increasingly extended because of their cost, size, robustness and power consumption. However, the effectiveness of the AIS algorithms is compromised by using them when there is a null drift along the time, which is a very common issue mainly in gyroscopes [25,26]. For a standard crane application, this major drawback could be avoided with a frequent time-basis calibration of the gyroscope, but it is not a feasible solution.

The novelty approach presented in this manuscript focuses on the development of an automatic compensation of this drift to obviate such frequent calibrations. It follows an analog development to that of the algebraic non-asymtotic parameter identification[24], by adding the null drift of the sensor as a new parameter to be identified. This AIS method is able to converge in less than half of the oscillation period and does not require defining initial conditions and, hence, it could be adequate to control the swaying of a crane in single maneuvers, where no learning

process is provided.

The novelty approach proposed overcomes some limitations of other AIS methods in our current application field. Within them, the Time-varying transfer function estimation (TTFE) uses an algorithm in the frequency domain to identify the system parameters [20]. Nevertheless, several oscillation periods are required to converge, making it impractical for short maneuvers. Other techniques use the time domain to achieve a solution. Nonetheless, some limitations to use them on cranes are pointed out, such as the estimation of the parameters requires that the maneuver has ended [21], or the solid-rigid position is not guaranteed unless the parameters are calculated between maneuvers [22]. Based on a LIS identification [18], a solution to update the parameters during the motion is presented [23]. However, some initial conditions are required and the estimation algorithm does not work in any part of the command input, which implies losing efficiency on the convergence.

The rest of this manuscript is organized as follows. In Section 2, the problem formulation is introduced assuming a one degree-of-freedom damped linear system with a constant parameter motion equation. It is shown the noticeable effect of the null drift of the feedback sensor on the estimation errors. In Section 3, the modified adaptive algorithm is explained. In Section 4, some experimental results are shown by using a pendulum-carriage test bed in a real time scenario. Finally, in Section 5, conclusions are drawn, pointing out the benefits of the method developed.

2. Problem formulation

The development carried out in this section follows that of an algebraic non-asymptotic parameter identification [24], and assumes a ZV shaper (two impulses) to benefit from shorter command durations when an adaptive algorithm is used. Nevertheless, it can be easily extended to more robust input shapers. The basic block diagram of an adaptive scheme is presented in Figure 1.

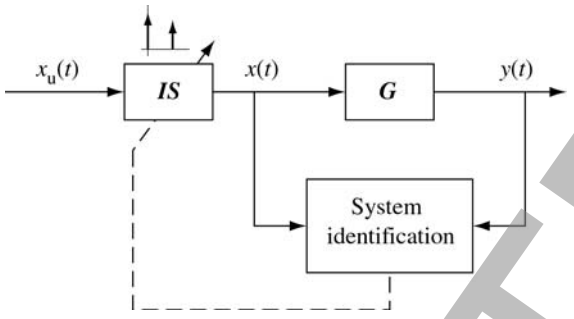

Fig. 1 Block diagram of an adaptive input shaper: ***IS*** is the input shaper and ***G*** is the oscillatory system

The vibratory system is described by a second order harmonic oscillator, in which $x(t)$ is the input and $y(t)$ is the system response. The transfer function $\boldsymbol{G}(s)$, the corresponding second order differential equation and the response of the system $y_h(t)$ to an impulse of magnitude A are, respectively:

$$\boldsymbol{G}(s)=\frac{\boldsymbol{Y}(s)}{\boldsymbol{X}(s)}=\frac{\omega_0^2}{s^2+2\zeta\omega_0 s+\omega_0^2} \tag{1}$$

$$\ddot{y}(t)+2\zeta\omega_0\dot{y}(t)+\omega_0^2 y(t)=\omega_0^2 x(t) \tag{2}$$

$$y_h(t)=\frac{A\omega_0}{\sqrt{1-\zeta^2}}e^{-\zeta\omega_0 t}\sin(\omega_d t) \tag{3}$$

where $\omega_d=\omega_0\sqrt{1-\zeta^2}$ is the oscillation frequency, ω_0 is the natural frequency and ζ is the damping ratio.

The transfer function of a ZV input shaper can be written as:

$$\boldsymbol{IS}(s)=\frac{X(s)}{\boldsymbol{X}_u(s)}=\frac{1}{1+K}+\frac{K}{1+K}e^{\frac{\pi}{\omega_d}s} \tag{4}$$

$$K = \mathrm{e}^{\left(\frac{-\zeta\pi}{\sqrt{1-\zeta^2}}\right)} \qquad (5)$$

The first addend of the expression (4) corresponds to an impulse located at t_1=0 and module $A_1 = 1/(1+K)$. The second addend is the second impulse at $t_2 = \pi/\omega_\mathrm{d}$ and module $A_2 = K/(1+K)$.

During the motion, the sensor provides feedback of the system response $y(t)$ to the identification algorithm. With this information, ω_0 and ζ are estimated in real time, and the sequence of impulses can be properly defined to reduce residual vibrations.

Assume that the feedback sensor provides a velocity signal $\dot{y}(t)$. If the basic algorithm[24] is formulated, the equation (2) yields:

$$\eta_1(t) + 2\zeta\omega_0\eta_2(t) + \omega_0^2\eta_3(t) = 0 \qquad (6)$$

where

$$\begin{aligned}
\eta_1(t) &= -t\,\dot{y}(t) + \int_0^t \dot{y}(\sigma)\mathrm{d}\sigma \\
\eta_2(t) &= -\int_0^t \sigma\,\dot{y}(\sigma)\mathrm{d}\sigma \qquad (7)\\
\eta_3(t) &= -\int_0^t\int_0^\sigma\int_0^\lambda \dot{y}(\rho)\mathrm{d}\rho\mathrm{d}\lambda\mathrm{d}\sigma - \int_0^t\int_0^\sigma \lambda\,\dot{y}(\lambda)\mathrm{d}\lambda\mathrm{d}\sigma + \int_0^t \sigma x(\sigma)\mathrm{d}\sigma
\end{aligned}$$

A second equation is obtained by integrating equation (6) and, hence, the terms ω_0^2 and $2\zeta\omega_0$ are derived:

$$\omega_0^2 = \frac{\eta_1(t)\int_0^t\eta_2(\sigma)\mathrm{d}\sigma - \eta_2(t)\int_0^t\eta_1(\sigma)\mathrm{d}\sigma}{\eta_2(t)\int_0^t\eta_3(\sigma)\mathrm{d}\sigma - \eta_3(t)\int_0^t\eta_2(\sigma)\mathrm{d}\sigma} \qquad (8)$$

$$2\zeta\omega_0 = \frac{\eta_3(t)\int_0^t\eta_1(\sigma)\mathrm{d}\sigma - \eta_1(t)\int_0^t\eta_3(\sigma)\mathrm{d}\sigma}{\eta_2(t)\int_0^t\eta_3(\sigma)\mathrm{d}\sigma - \eta_3(t)\int_0^t\eta_2(\sigma)\mathrm{d}\sigma} \qquad (9)$$

2.1 Effect of the null drift

Although the null drift is a function of time, in this study it is taken as an unknown constant because the timeframe in which the adaptive algorithm is processed is very short. The measurement from the sensor $v(t)$ yields:

$$v(t) = \dot{y}(t) + v_\mathrm{d} \qquad (10)$$

where $\dot{y}(t)$ is the real velocity and v_d is the null drift at a certain time. By substituting (10) in (2) we obtain:

$$\dot{v}(t) + 2\zeta\omega_0\left(v(t) - v_\mathrm{d}\right) + \omega_0^2\int_0^t\left(v(\sigma) - v_\mathrm{d}\right)\mathrm{d}\sigma = \omega_0^2 x(t) \qquad (11)$$

Applying the referenced algorithm, the Laplace transform of (11) yields:

$$s\boldsymbol{V}(s) - v(0) + 2\zeta\omega_0\left[\boldsymbol{V}(s) - \frac{1}{s}v_\mathrm{d}\right] + \omega_0^2\left[\frac{1}{s}\boldsymbol{V}(s) - \frac{1}{s^2}v_\mathrm{d}\right] = \omega_0^2\boldsymbol{X}(s) \qquad (12)$$

Equation (12) is derived with regard to s and divided by s:

$$\frac{1}{s}\boldsymbol{V} + \frac{\mathrm{d}\boldsymbol{V}}{\mathrm{d}s} + 2\zeta\omega_0\left[\frac{1}{s}\frac{\mathrm{d}\boldsymbol{V}}{\mathrm{d}s} + \frac{1}{s^3}v_\mathrm{d}\right] + \omega_0^2\left[-\frac{1}{s^3}\boldsymbol{V} + \frac{1}{s^2}\frac{\mathrm{d}\boldsymbol{V}}{\mathrm{d}s} + \frac{2}{s^4}v_\mathrm{d}\right] = \frac{\omega_0^2}{s}\frac{\mathrm{d}\boldsymbol{X}}{\mathrm{d}s} \qquad (13)$$

The inverse of the Laplace transform is applied to (13) and results in the time-domain equation (14), where it is showed a noticeable effect of v_d because of the time exponents of the extra addends.

$$\eta_1(t) + 2\zeta\omega_0\eta_2(t) + \omega_0^2\eta_3(t) + \zeta\omega_0 v_d t^2 + \frac{1}{3}\omega_0^2 v_d t^3 = 0 \qquad (14)$$

Assume that $\hat{\omega}_0$ and $\hat{\zeta}$ are the estimations of ω_0 and ζ, respectively. The errors on these estimators can be defined by:

$$\text{error } \omega_0 = \frac{\hat{\omega}_0 - \omega_0}{\omega_0} \qquad (15)$$

$$\text{error } \zeta = \frac{\hat{\zeta} - \zeta}{\zeta} \qquad (16)$$

Figure 2 depicts these errors with regard to the null drift of the feedback device v_d, when this null drift is not considered. The example used is an oscillator of 1 Hz of natural frequency, with 0.05 and 0.1 damping ratios. The input $x(t)$ used is a single impulse of magnitude A and $\hat{\omega}_0$ and $\hat{\zeta}$ have been evaluated at $t_2 = \pi/(\omega_0\sqrt{1-\zeta^2})$ (approximately 0.5 s), which is the ideal location of the second impulse. The null drift scale has been normalized by the maximum amplitude of the velocity response, $A\omega_0^2/\sqrt{1-\zeta^2}$, derived from equation (3).

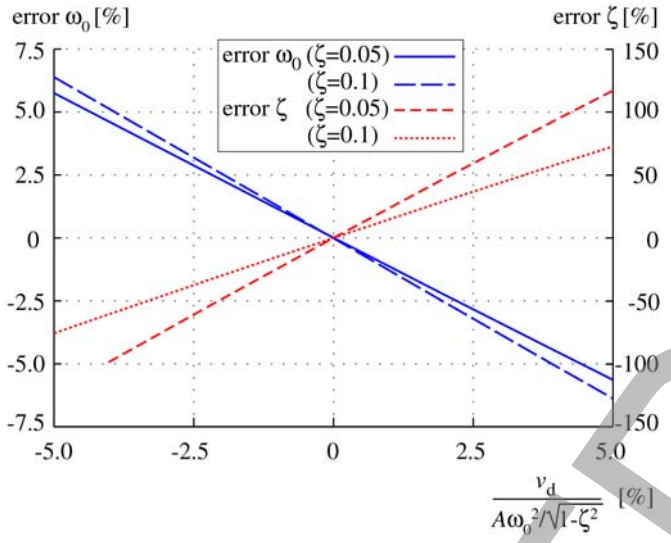

Fig. 2 Error on the estimation of natural frequency and damping ratio versus de null drift of the feedback device

2.2 Single maneuvers

The consequence of the drift v_d can be expressed in terms of residual vibration when the adaptive ZV input shaper is used. However, some thoughts must be introduced when this algorithm is applied in single maneuvers, which is the usual situation in cranes.

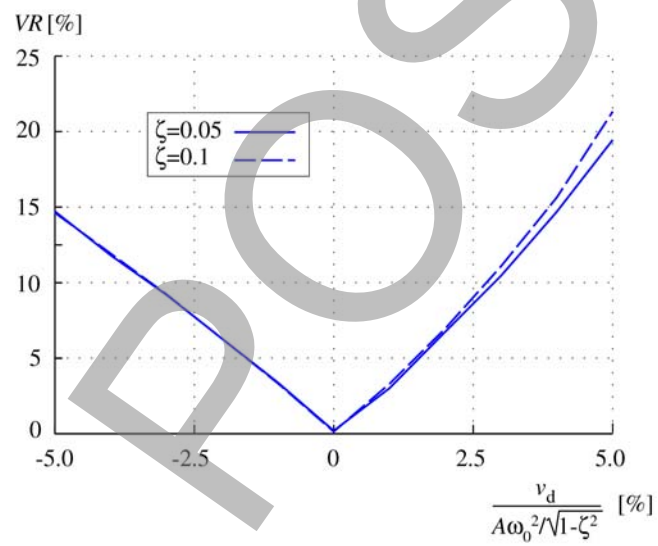

Fig.3 Residual vibration versus the null drift of the feedback device

Consider the system of the former example, now with a ZV shaper. The first impulse is located at $t_1 = 0$. Its amplitude, $A_1 = 1/(1+K)$, must be presumed without knowing the damping ratio of the system (required to calculate K) because we are supposing that the system is completely unknown. Consequently, once A_1 is guessed, the amplitude of the second impulse A_2 is automatically preset to maintain the condition of rigid body motion of the shaper, i.e., $A_1 + A_2 = 1$. Therefore, $\hat{\zeta}$ can only be used to estimate the location of the second impulse $\hat{t}_2 = \pi/(\hat{\omega}_0\sqrt{1-\hat{\zeta}^2})$. With this hypothesis, the equation (17) describes the percentage of residual vibration [13] for a given $\hat{t}_2(\hat{\omega}_0, \hat{\zeta})$, assuming ideal A_1 and A_2. Figure 3 shows the graphical result, where it can be seen that a small null drift implies a noticeable effect on the residual vibration.

$$VR(\hat{t}_2) = \mathrm{e}^{-\zeta\omega_0\hat{t}_2}\sqrt{\left(A_1 + A_2\mathrm{e}^{\zeta\omega_0\hat{t}_2}\cos\left(\omega_\mathrm{d}\hat{t}_2\right)\right)^2 + \left(A_2\mathrm{e}^{\zeta\omega_0\hat{t}_2}\sin\left(\omega_\mathrm{d}\hat{t}_2\right)\right)^2} \qquad (17)$$

3. Modified adaptive algorithm

To improve this poor estimation, it is proposed to modify the current algorithm by introducing the null drift v_d as a new parameter to be identified. From equation (14), it is proposed the following array to be identified:

$$\boldsymbol{q} = \left\{2\zeta\omega_0 \;\; \omega_0^2 \;\; \zeta\omega_0 v_\mathrm{d} \;\; \frac{1}{3}\omega_0^2 v_\mathrm{d}\right\}^\mathrm{T} \qquad (18)$$

Following the same procedure to that of the former algorithm, three more equations are obtained by integrating equation (14):

$$\int_0^t \eta_1(\sigma)\mathrm{d}\sigma + 2\zeta\omega_0\int_0^t \eta_2(\sigma)\mathrm{d}\sigma + \omega_0^2\int_0^t \eta_3(\sigma)\mathrm{d}\sigma + \zeta\omega_0 v_\mathrm{d}\frac{t^3}{3} + \frac{1}{3}\omega_0^2 v_\mathrm{d}\frac{t^4}{4} = 0 \qquad (19)$$

$$\int_0^t\int_0^\sigma \eta_1(\lambda)\mathrm{d}\lambda\mathrm{d}\sigma + 2\zeta\omega_0\int_0^t\int_0^\sigma \eta_2(\lambda)\mathrm{d}\lambda\mathrm{d}\sigma + \omega_0^2\int_0^t\int_0^\sigma \eta_3(\lambda)\mathrm{d}\lambda\mathrm{d}\sigma + \zeta\omega_0 v_\mathrm{d}\frac{t^4}{12} + \frac{1}{3}\omega_0^2 v_\mathrm{d}\frac{t^5}{20} = 0 \qquad (20)$$

$$\int_0^t\int_0^\sigma\int_0^\lambda \eta_1(\rho)\mathrm{d}\rho\mathrm{d}\lambda\mathrm{d}\sigma + 2\zeta\omega_0\int_0^t\int_0^\sigma\int_0^\lambda \eta_2(\rho)\mathrm{d}\rho\mathrm{d}\lambda\mathrm{d}\sigma + \omega_0^2\int_0^t\int_0^\sigma\int_0^\lambda \eta_3(\rho)\mathrm{d}\rho\mathrm{d}\lambda\mathrm{d}\sigma + \zeta\omega_0 v_\mathrm{d}\frac{t^5}{60} + \frac{1}{3}\omega_0^2 v_\mathrm{d}\frac{t^6}{120} = 0 \qquad (21)$$

A system of equations with the form $\boldsymbol{A}\boldsymbol{q} = \boldsymbol{q}_0$ can be made up with (14), (19), (20) and (21). Its solution yields:

$$\boldsymbol{q} = \boldsymbol{A}^{-1}\boldsymbol{q}_0 \qquad (22)$$

where $\boldsymbol{A}$ and $\boldsymbol{q}_0$ are:

$$A = \begin{bmatrix} \eta_2 & \eta_3 & t^2 & t^3 \\ \int_0^t \eta_2\mathrm{d}\sigma & \int_0^t \eta_3\mathrm{d}\sigma & \frac{t^3}{3} & \frac{t^4}{4} \\ \int_0^t\int_0^\sigma \eta_2\mathrm{d}\lambda\mathrm{d}\sigma & \int_0^t\int_0^\sigma \eta_3\mathrm{d}\lambda\mathrm{d}\sigma & \frac{t^4}{12} & \frac{t^5}{20} \\ \int_0^t\int_0^\sigma\int_0^\lambda \eta_2(\rho)\mathrm{d}\rho\mathrm{d}\lambda\mathrm{d}\sigma & \int_0^t\int_0^\sigma\int_0^\lambda \eta_3(\rho)\mathrm{d}\rho\mathrm{d}\lambda\mathrm{d}\sigma & \frac{t^5}{60} & \frac{t^6}{120} \end{bmatrix} \qquad (23)$$

$$\boldsymbol{q}_0 = \begin{Bmatrix} -\eta_1 \\ -\int_0^t \eta_1\mathrm{d}\sigma \\ -\int_0^t\int_0^\sigma \eta_1\mathrm{d}\lambda\mathrm{d}\sigma \\ -\int_0^t\int_0^\sigma\int_0^\lambda \eta_1\mathrm{d}\rho\mathrm{d}\lambda\mathrm{d}\sigma \end{Bmatrix} \qquad (24)$$

A drawback in terms of fastness on the convergence of the proposed algorithm must be pointed out due to the fact of obtaining three extra equations by integrating (14). This issue compromises the goodness of the method by increasing the residual vibration. To cope with this slowness, it is proposed to eliminate the last equation and solve for the unknowns ω_0, ζ and v_d the resultant non-linear system (equations (14), (19) and (20)). Now it is assumed the system of the former example with 0.1 damping ratio. Figure 4 shows the fastest convergence of $\hat{\omega}_0$ and $\hat{\zeta}$ at the ideal $t_2 = \pi/(\omega_0\sqrt{1-\zeta^2}) \approx 0.5$ s, when this second approach is used.

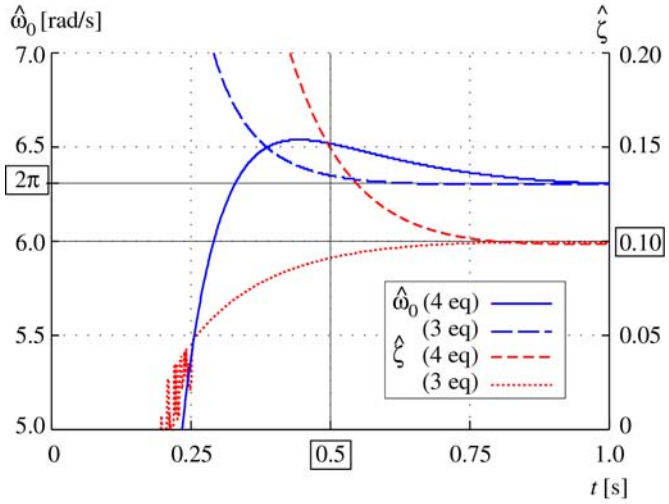

Fig.4 Convergence of the estimated parameters $\hat{\omega}_0$ and $\hat{\zeta}$ by solving with a linear system (4 equations) and with a non-linear system (3 equations)

3.1 Lightly damped systems

In most of the vibratory systems, where the damping is not particularly enforced, the damping ratio is usually very small. This situation is especially noticeable in cranes [27], where it takes values around 0.01. In this case, the damping ratio identification in single maneuvers becomes difficult, where small perturbations, such as signal noise, can lead to significant errors. For example, the induced error in residual vibration when considering whether or not a damping ratio of $\zeta = 0.01$ is around 1.5%. Therefore, it is suggested to obviate the identification of this parameter and, hence, reduce the number of equations to two (equations (14) and (19)) which, in turn, could compensate the error mentioned by obtaining a faster convergence in the estimation of ω_0 and v_d.

4. Experimental results

Fig. 5 Carriage-pendulum test platform: 1) pendulum, 2) gyroscope, 3) carriage

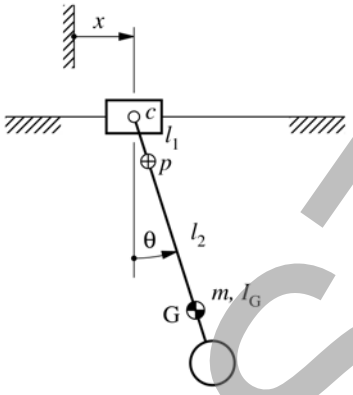

Fig. 6 Pendulum schematics and coordinates

The carriage-pendulum test bed of Figure 5 was built to check the goodness of the proposed method. The pendulum with planar motion, which represents essentially a crane, is described by the schematics of the Figure 6, where the mass m, the inertia I_G, the gyroscope p and the lengths l_1 and l_2 are depicted. The rod is articulated on the carriage and the internal friction loss is formulated by a rotary damper with damping constant c. The carriage displacement is defined by the coordinate x and follows a command input driven with a control, a DC motor and a belt-pulley transmission. The feedback for this control is provided by an incremental rotary encoder, which measures the carriage displacement through the angular position of the idler pulley. The pendulum angle is defined by the coordinate θ and the angular velocity is measured by means of a MEM gyroscope integrated circuit that is assembled on the rod near to the pendulum rotary axis.

Table 1 shows a summary of the values and devices of this test bed.

Table 1 Test bed parameters and specifications

Parameter / device	Value / specification
m	0.797 kg
I_G	$15.8 \cdot 10^{-3}$ kg·m^2
l_1	30 mm
l_2	240 mm
c	$14.7 \cdot 10^{-3}$ Nm/(rad/s)
Motor	Permanent magnet DC brushed
Encoder	Rotary, 7200 cycles per revolution
Gyroscope p	ADXRS300, ±300º/s, 5mV/(º/s) Linear accel. effect 0.2 (º/s)/g
Power supply	DC 24V, 10A
Power electronics	Galil Motion Control MSA12-80
Control electronics	NI PCI-6036E
Control software	Matlab Simulink®
Computer	Xeon ®, 3.0 GHz, 3.25 GB RAM

The motion equation of this pendulum for a given $x(t)$ is described by:

$$(ml^2 + I_G)\ddot{\theta} + c\dot{\theta} + mgl\sin\theta = -m\ddot{x}(t)l\cos\theta \qquad (25)$$

Consider that the oscillations during and after the transient are small and around the position θ=0º. Therefore, the motion equation can be linearized as:

$$(ml^2 + I_G)\ddot{\theta} + c\dot{\theta} + mgl\theta = -m\ddot{x}(t)l \qquad (26)$$

This equation can be rewritten as:

$$\ddot{\theta} + 2\zeta\omega_0\dot{\theta} + \omega_0^2\theta = -\frac{\omega_0^2}{g}\ddot{x}(t) \qquad (27)$$

where the system natural frequency and the damping ratio are, respectively:

$$\omega_0 = \sqrt{\frac{mgl}{ml^2 + I_G}} \qquad (28)$$

$$\zeta = \frac{c}{2\sqrt{mgl(ml^2 + I_G)}} \qquad (29)$$

The test-bed setup gives a measured oscillation frequency of ω_d=5.342 rad/s and a damping ratio of ζ=0.019. Therefore, the system natural frequency obtained by calculation is ω_0=5.343 rad/s. The bandwidths of the motor-carriage system and the electronics have cut-off frequencies that are far from the system resonance and, hence, their filtering effect is not significant.

The gyroscope voltage output $V_{out}(t)$ gives values between 0 to 5 volts, and can be transformed to the angular velocity $v(t)$ through the expression:

$$v(t) = \frac{V_{out}(t) - V_{offset}}{s} \qquad (30)$$

where V_{offset} is the nominal voltage offset (2.5 V) and s is the device sensitivity (5mV/(º/s)). Once the angular velocity is available, and assuming rest initial conditions, the angular position is obtained by discrete time integration with Euler's method. Similarly to the expression (10), we can describe the gyroscope measurement $v(t)$ as the sum of the real angular velocity $\dot{\theta}(t)$ plus the null drift v_d:

$$v(t) = \dot{\theta}(t) + v_d \qquad (31)$$

If $v(t)$ is introduced in the equation (27), a similar equation than (11) can be written:

$$\dot{v}(t)+2\zeta\omega_0\left(v(t)-v_\mathrm{d}\right)+\omega_0^2\int_0^t\left(v(\sigma)-v_\mathrm{d}\right)\mathrm{d}\sigma=-\frac{\omega_0^2}{\mathrm{g}}\ddot{x}(t) \quad (32)$$

The rest of the development is analogous to that of the second order oscillator.

Two types of tests are carried out. The former test (Figure 7) shows the convergence of $\hat{\omega}_0$ versus time, when both the original algorithm (without taking into account the drift) and the modified one are used. In this last case, the estimation of ζ has been obviated as explained in 3.1. The tested maneuver is a point-to-point motion described by a versine function as the carriage velocity $\dot{x}(t)$. In the same Figure, the convergence of $\hat{v}_\mathrm{d}$ is showed as well. In this case the null drift of the gyroscope was set to $v_\mathrm{d}=0.15$ rad/s. Results show that, for the modified algorithm, the convergence is stable before the target measurement point at $t_2=\pi/(\omega_0\sqrt{1-\zeta^2})\approx 0.59$ s, and the values obtained are $\hat{\omega}_0=5.34$ rad/s and $\hat{v}_\mathrm{d}=0.16$ rad/s, which are quite close to the theoretical values $\omega_0=5.342$ rad/s and $v_\mathrm{d}=0.15$ rad/s. For the original algorithm, this convergence is not stable and the value obtained at the target measurement point ($\hat{\omega}_0=5.05$ rad/s) is far from the theoretical value.

The second test (Figure 8) compares the residual vibration obtained with regard to the null drift of the gyroscope, v_d, when the original algorithm and the modified one are used. In both cases, a versine function was chosen for the unshaped command $\dot{x}(t)$. Three sample tests have been performed for each v_d for both, the original and the modified algorithm. Results show the goodness of the method used, with a residual vibration 5 and 2 times lower when v_d is –0.15 rad/s and 0.15 rad/s, respectively.

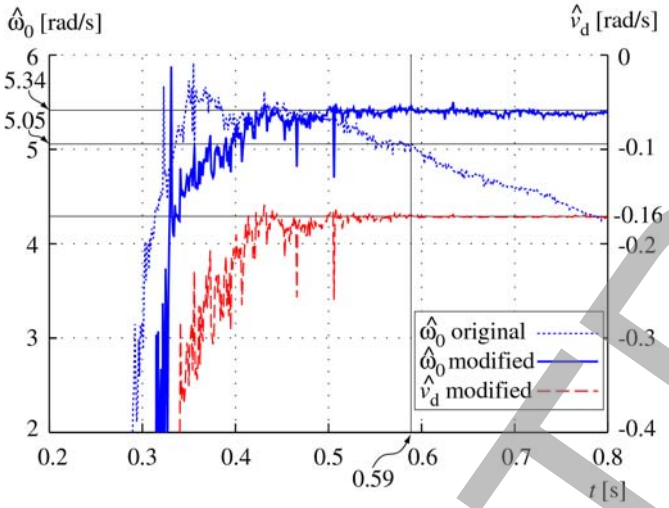

Fig. 7 Experimental results: convergence of $\hat{\omega}_0$ and $\hat{v}_\mathrm{d}$ versus time.

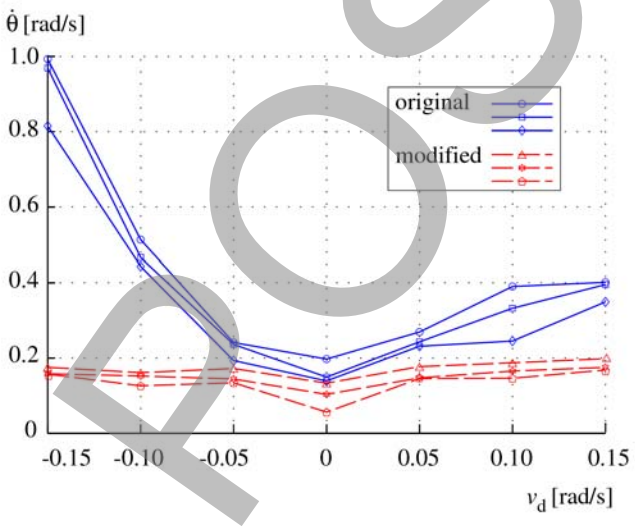

Fig. 8 Experimental results: Residual vibration $\dot{\theta}(t)$ versus the null drift of the gyroscope v_d, for the original adaptive algorithm and the modified one.

5. Conclusions

This paper presents an adaptive algorithm to reduce residual vibrations when the feedback sensor used has the drawback of having null drift along the time. The study focuses in single maneuvers of cranes and, hence, a large variation of the system parameters is foreseen, and a short convergence time is required. To deal with these constraints, the algorithm chosen is based on an algebraic non-asymptotic parameter identification, which is able to converge in less than half of the oscillation period and does not require defining initial conditions. Nevertheless, the null drift of the feedback sensor which is very common in MEM gyroscopes has a noticeable negative effect on the residual vibration. The proposed workaround follows an analog development to that of the original algorithm, but modifies it by including the null drift as a new parameter to be identified and, therefore, it can be compensated automatically. Moreover, in the case of lightly damped systems, such as a crane, it is suggested to obviate the estimation of the damping ratio and, hence, the fastness of the convergence is improved. A pendulum test bed, which is essentially a crane, is used to conduct some experiments with different setups of the null drift of the gyroscope and the results confirm the effectiveness and usefulness of the method.

REFERENCES

1. Singhose, W.E., “Command Shaping for Flexible Systems: A Review of the First 50 Years”, International Journal of Precision Engineering and Manufacturing, Vol. 10, No. 4, pp. 153-168, 2009.
2. Lim, S., Kim, K., Shim, J., Cha, K., Cho, C., “Torsional Vibration Control of the Rotating Chamber Using a Reaction Wheel,” International Journal of Precision Engineering and Manufacturing, Vol. 13, No. 6, pp. 891-897, 2012.
3. Veciana, J.M., Cardona, S., ” Residual Vibration Reduction in Mechanical Systems: A Time-domain Approach,” International Journal of Precision Engineering and Manufacturing, Vol. 13, No. 8, pp. 1327-1339, 2012.
4. Starr, G. P. "Swing-Free Transport of Suspended Objects with a Path-Controlled Robot Manipulator," ASME Journal of Dynamic Systems, Measurement, and Control, Vol. 107, No. 1, pp. 97-100, 1985.
5. Sorensen, K., Singhose, W., Dickerson, S., "A Controller Enabling Precise Positioning and Sway Reduction in Bridge and Gantry Cranes," Control Engineering Practice, Vol. 15, No. 7, pp. 825-837, 2007.
6. Kim, D., Singhose, W., "Performance Studies of Human Operators Driving Double-Pendulum Bridge Cranes," Control Engineering Practice, Vol. 18, No. 6, pp. 567-576, 2010.
7. Stergiopoulos, J., Konstantopoulos, G., Tzes, A., "Experimental Verification of an Adaptive Input Shaping Scheme for Hoisting Cranes," Mediterranean Conference on Control and Automation, pp. 730-735, 2009.
8. Veciana, J.M., Cardona, S., Català, P., ” Minimizing Residual Vibrations for Non-zero Initial States: Application to an Emergency Stop of a Crane,” International Journal of Precision Engineering and Manufacturing, Vol. 14, No. 11, pp. 1901-1908, 2013.
9. Tuan, L.A., Kim, J.-J., Lee, S.-G., Lim, T.-G., Nho, L.C., “Second-order Sliding Mode Control of a 3D Overhead Crane with Uncertain System Parameters,” International Journal of Precision Engineering and Manufacturing, Vol. 15, No. 5, pp. 811-819, 2014.
10. Tuan, L.A., Lee, S.-G., Nho, L.C., Kim, D.H., “Model Reference Adaptive Sliding Mode Control for Three Dimensional Overhead Cranes,” International Journal of Precision Engineering and Manufacturing, Vol. 14, No. 8, pp. 1329-1338, 2013.
11. Le, T.A., Lee, S.-G., Moon, S.-C., “Partial Feedback Linearization and Sliding Mode Techniques for 2D Crane Control,” International Journal of Precision Engineering and Manufacturing, Vol. 13, No. 4, pp. 501-507, 2012.
12. Smith, O. J. M., “Posicast Control of Damped Oscillatory Systems,” Proc. The IRE, Vol. 45, No. 9, pp.1249-1255, 1957.
13. Singer, N.C., Seering, W.P., “Preshaping Command Inputs to Reduce System Vibration”, ASME Journal of Dynamic Systems, Measurement, and Control, Vol. 112, No. 1, pp. 76-82, 1990.
14. Hyde, J.M., Seering, W.P., “Using Input Command Pre-Shaping to Suppress Multiple Mode Vibration”, IEEE Proceedings of the International Conference on Robotics and Automation, pp. 2604-2609, 1991.
15. Hyde, J.M., Seering, W.P., "Inhibiting Multiple Mode Vibration in Controlled Flexible Systems," Proceedings of the American Control Conference, pp. 2449-2454, 1991.
16. Singhose, W.E., Seering, W.P., Singer, N.C., “Residual Vibration Reduction Using Vector Diagrams to Generate Shaped Inputs”, ASME

Journal of Mechanical Design, Vol. 116, pp. 654-659, 1994.

17. Singhose, W.E., Porter, L.J., Tuttle, T.D. and Singer, N.C., "Vibration Reduction Using Multi-Hump Input Shapers", ASME Journal of Dynamic Systems, Measurement, and Control, Vol. 119, No. 2, pp. 320-326, 1997.
18. Park, J., and Chang, P. H., "Learning Input Shaping Technique for Non-LTI Systems", ASME Journal of Dynamic Systems, Measurement, and Control, Vol. 123, No. 2, pp. 288-293, 2001.
19. Park, J., Chan, P. H., Park, H. S. and Lee, E., "Design of Learning Input Shaping Technique for Residual Vibration Suppression in an Industrial Robot", IEEE/ASME Transactions on Mechatronics, Vol. 11, No. 1, pp. 55-65, 2006.
20. Tzes, A. and Yurkovich, S., "An Adaptive Input Shaping Control Scheme for Vibration Reduction Suppression in Slewing Flexible Structures", IEEE Transactions on Control Systems Technology, Vol. 1, No. 2, pp. 114-121, 1993.
21. Rhim, S. and Book, W. J., "Noise Effect on Adaptive Command Shaping Methods for Flexible Manipulator Control", IEEE Transactions on Control System Technology, Vol. 9, No. 1, pp. 84-92, 2001.
22. Bodson, M., "An Adaptive Algorithm for the Tuning of Two Input Shaping Methods", Automatica, Vol. 34, No 6, pp. 771-776, 1998.
23. Cutforth, C. F. and Pao, L. Y., "Adaptive Input Shaping for Manoeuvring Flexible Structures", Automatica, Vol. 40, No. 4, pp. 685-693, 2004.
24. Pereira, E., Trapero, J.R., Díaz, I.M. and Feliu, V. "Adaptive Input Shaping for Manoeuvring Flexible Structures Using an Algebraic Identification Technique", Automatica, Vol. 45, No. 4, pp. 1046-1051, 2009.
25. Weinberg, M.S. and Kourepenis, A., "Error Sources in In-Plane Silicon Tuning-Fork MEMS Gyroscopes", Journal of Microelectromechanical Systems, Vol. 15, No. 3, pp. 479-491, 2006.
26. Prikhodko, I.P., Trusov, A.A. and Shkel, A.M., "Compensation of Drifts in High-Q MEMS gyroscopes Using Temperature Self-Testing", Sensors and Actuators A: Physical, Vol. 201, pp. 517-524, 2013.
27. Ely, P.T., "Internal Damping Rates of Construction Cranes", Master Thesis, Virginia Polytechnic Institute and State University, 1997.